Microscopy, 2023, **72(2)**, 135–143
DOI: https://doi.org/10.1093/jmicro/dfac053
Advance Access Publication Date: 21 October 2022
Special Issue Paper

MICROSCOPY

Progress in spatial resolution of structural analysis by cryo-EM

Yoshiyuki Fukuda[1,*], **Kevin Stapleton**[2] and **Takayuki Kato**[2,*]

[1]Department of Cell Biology and Anatomy, Graduate School of Medicine, The University of Tokyo, Bunkyo, Tokyo 113-0033, Japan
[2]Institute for Protein Research, Osaka University, Suita, Osaka, 565-0871, Japan
[*]To whom correspondence should be addressed. E-mail: fukuday@m.u-tokyo.ac.jp (Y.F.); tkato@protein.osaka-u.ac.jp (T.K.)

Abstract

Since the Human Genome Project, drug discovery via structure-based drug design and development has significantly accelerated. Therefore, generating high-resolution structural information from biological macromolecules and macromolecular complexes, such as proteins and nucleic acids, is paramount in structural biology, medicine and the pharmaceutical industry. Recently, electron cryomicroscopy (cryo-EM) has undergone a technological revolution and attracted much attention in the structure-based drug discovery pipeline. This recognition is primarily due to its ability to analyze and reconstruct high-resolution structures of previously unattainable large target macromolecular complexes captured in various functional and dynamic states. Previously, cryo-EM was a niche method in the structure determination field, and research was limited to a small number of laboratories and produced low-resolution structures incomplete for detailed and unambiguous structural interpretation. However, with the development of new camera technology, software and computational algorithms that now seamlessly integrate these new developments, the achievable resolutions produced from cryo-EM–determined structures have dramatically improved. This has solidified cryo-EM as one of the main structural determination methods widely used in the field. In this review, we introduce the evolution of two essential techniques incorporated into the cryo-EM workflow—single particle analysis and tomography—focusing on achievable resolution and the technological innovations that have become indispensable tools for high-resolution reconstruction and structural analysis of biological macromolecules. Here, we also describe challenges and discuss future prospects that have fixed cryo-EM as a dominant feature in the landscape of high-resolution structure determination methods and the structure-based drug discovery pipeline.

Key words: cryo-EM, high resolution, single particle analysis, cryo-electron tomography, subtomogram averaging

Introduction

Biological macromolecules such as proteins or nucleic acids carry out various essential biological functions within a cell. In structural biology, the link between a macromolecule's three-dimensional (3D) structure and its function is referred to as the structure–function relationship. This relationship not only provides a deeper understanding of the function and biological activity of biological macromolecules within the context of the cell, but additionally, the structural information is essential for drug design [1]. However, revealing the 3D structure of a macromolecule at near-atomic resolutions requires the analysis of raw images containing sufficient spatial resolution with proper procedures.

Recent technological breakthroughs in electron cryomicroscopy (cryo-EM) and innovations from computational and methodological approaches have brought about a 'resolution revolution' in the field of structural biology. Two distinguishing features of the cryo-EM method of structural analysis compared with other structural techniques, such as X-ray crystallography, are (i) it does not require a unique sample preparation or crystallization to analyze structures closer to their functional state, and (ii) it enables direct visualization of immobilized, biological macromolecules embedded in vitreous ice in their near-native conformations. In combination with new technologies, these features have promoted cryo-EM as one of the mainstream structure determination methods that can routinely obtain 3D structures of macromolecules or complex assemblies at resolutions routinely better than 4 Å.

There are three main techniques deployed for macromolecule structure determination and structural analysis techniques using cryo-EM: electron diffraction (including microcrystal electron diffraction), single particle analysis (SPA), and cryo-electron tomography (cryo-ET). Here, we present the resolution capabilities from two of these methods; the SPA approach—in which the resolution has been dramatically improved in recent years and has become a mainstay of structural analysis—and cryo-ET, which is the unique method that enables the structural analysis of macromolecular complexes functioning within a cell.

Structural analysis by SPA

Before camera

In the comparison with other structural analysis techniques such as X-ray crystallography and nuclear magnetic resonance (NMR), SPA cryo-EM does not require a crystallizable sample as is necessary for X-ray crystallography and can analyze larger macromolecular complexes unlike that of NMR. Therefore, SPA cryo-EM has access to a broader range of target macromolecular complexes and complex macromolecular assemblies available for 3D structural determination. However, despite these crucial features, SPA cryo-EM traditionally

Received 1 September 2022; Revised 13 October 2022; Editorial Decision 14 October 2022; Accepted 19 October 2022

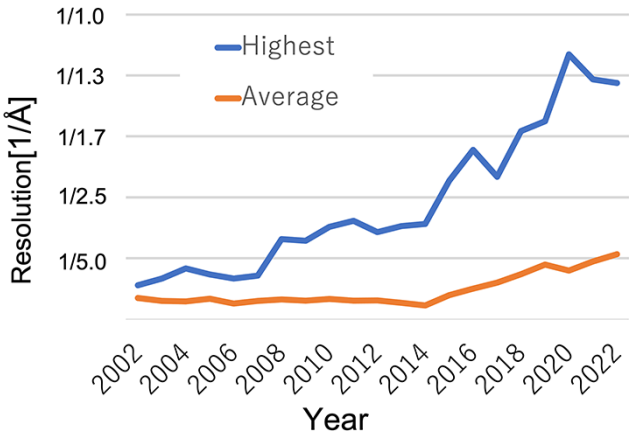

Fig. 1. The trend of the highest and average resolution by SPA in every year.

reported lower-resolution structures until about 10 years ago. Figure 1 illustrates the average and maximum resolution of structures derived from SPA to date. Before 2015, the average resolution was 15–20 Å. This resolution range is sufficient to identify a target macromolecule's overall structure and individual domains. However, secondary structures such as α-helices and β-sheets cannot be resolved at such a resolution, and therefore, the atomic models could not be built from the resulting EM coulomb density volumes (density maps) derived by SPA.

To address the issue of insufficient resolutions for modeling the atomic coordinates, the general approach was to perform a quasi-atomic resolution structural analysis. In this approach, the whole structure of the complex was analyzed by SPA producing a low- to an intermediate-resolution density map, and the subunits or local domains of the density map would be fitted with atomic coordinates previously determined by X-ray crystallography or NMR. In the early days of cryo-EM structural analysis, it was often derided as 'blobology' which is a combination of the words 'blob' and 'biology', because it produced low-resolution, nearly spherical, featureless density maps that could fit atomic models in any orientation.

After direct electron detector

Previously, target macromolecular images were recorded on film or conventional charge-coupled device (CCD)/complementary metal-oxide semiconductor (CMOS) cameras. The biggest drawback of the SPA approach at that time, i.e. the 3D reconstruction of low- and intermediate-resolution structures, was improved mainly by a new type of camera that detects electrons directly. In 2013, several impressive structural analysis articles using this new camera, called direct electron detector (DED), were published, demonstrating its immense effectiveness [2–4]. In 2015, the average resolution improved dramatically to about 6 Å as shown in Fig. 1. In the author's experience, at present, many biomolecules examined by SPA cryo-EM can now be analyzed and regularly reconstructed to resolutions around 2.5–4.5 Å. At near-atomic resolutions reported in this range, a typical user can not only build the atomic model of the main chain from the density map but also unambiguously register side chains.

The dawn of a new era brought about by the DED is named as the 'the resolution revolution' in 2014 [5]. Although the basic research on DEDs at that time had already demonstrated a higher detective quantum efficiency (DQE) and modulation transfer function (MTF) than conventional CCDs, scintillator and fiber optic CMOSs and photographic film, the appearance of the first DEDs did not bring about a dramatic change [6–9] at least in terms of the reported resolution. Actually, DEDs had already been commercially available since 2008, approximately 5 years before the first impressive paper about using DEDs for SPA.

One significant factor that contributes to the lack of high-resolution structures produced by the SPA cryo-EM early on, despite the advances in DED technology, was the sample movement in the ice layer induced by electron beam irradiation, which is called 'beam-induced motion' [10,11]. The beam-induced motion of particles in ice eliminates higher-resolution information more so than the DQE and MTF of the camera. Therefore, the beam-induced motion was considered one of the most important factors limiting the achievable resolutions of SPA structures and resulted in the exploration of many potential solutions [12–17]. One very effective solution significantly curbing the seemingly intractable problem of beam-induced motion was the capability of DEDs to record movies with a fast frame rate.

All current DEDs made of CMOS sensors record information projected on the detector with a high frame rate. Therefore, DEDs can also record the data not as a single image, as is the case with conventional cameras or film, but as moving frames. Even if the sample moves in ice due to the beam-induced motion, each frame recorded in the movie can be aligned computationally during image analysis to produce a sharp, blur-free single image. The process of correction for beam-induced motion is called 'motion correction' [2,18–20], and combined with the detector's sensitivity, motion correction has dramatically improved the achievable resolutions produced by SPA.

World records for resolution

The highest resolution of structural analysis using film was published by Yu *et al.* in 2011 of a 3.1 Å resolution cytoplasmic polyhedrosis virus [21]. By contrast, the first example of the highest resolution using a DED was a 2.8 Å resolution structure of 20S proteasome by Campbell *et al.* in 2015 [22]. This result was the highest resolution at that time, and the first example beyond 3 Å using SPA cryo-EM. In the same year, Grant *et al.* determined the structure of rotavirus VP6 at 2.6 Å resolution [23], and the world record for resolution was broken. In this article, the estimation of optimal exposure values and filtering movie frames using these values was carefully analyzed to showcase the advantages of movies recorded by DEDs. This filtering, called 'dose weight', is now a standard protocol for high-resolution structural analysis, as is motion correction. Shortly thereafter, Bartesaghi *et al.* in 2016 published the structure of b-galactosidase at 2.2 Å resolution [24]. Surprisingly, from this resolution, the holes from aromatic ring side chains, such as phenylalanine and tryptophan, could be visualized in the density map.

The 2.2 Å structure of b-galactosidase provided the first significant indication that SPA, as a tool for near-atomic resolution structural determination, was now assembling structures close to the average resolution of those produced from X-ray crystallography. Furthermore, in 2016, Merk *et al.* were the first to demonstrate that SPA could bring structures

to atomic resolutions (better than 2 Å) by reconstructing the structure of glutamate dehydrogenase (GDH) at 1.8 Å resolution [25].

Next, Zivanov *et al.* successfully performed the structural analysis of a 1.65 Å resolution structure of apoferritin in July 2018. This investigation was a test sample for the development of the latest version, v3.0 of RELION, currently the most popular structural analysis software available. Zivanov *et al.* reported their 1.65 Å in resolution result to the world via Twitter before publishing the article, breaking the previous world record GDH at 1.8 Å in resolution [26]. However, on the same day, Danev *et al.* also reported the structural analysis of apoferritin at 1.62 Å resolution via Twitter, thereby the world record was broken in the same day [27]. Later, in October 2018, Yoshioka *et al.* announced on Twitter that they had achieved a resolution of 1.56 Å for the adeno-associated virus (AAV) structure [28]. Their AAV is the only example other than apoferritin that has been successfully analyzed to resolutions higher than 1.7 Å. In 2019, Kato *et al.* succeeded in analyzing the structure of 1.54 Å resolution structure of apoferritin [29]. In addition to the highest resolution at the time, the data by Kato *et al.* were unique in that the data were obtained using the latest JEOL electron cryomicroscope (CRYOARM300), instead of the Titan Krios from Thermo Fisher Scientific, which has cornered the market as the cryo-EM instrument of choice, and given the users a new option. The CRYOARM300 is the first cryo-EM to install the cold field emission gun (cold-FEG) [30]. The energy spread of the cold-FEG is approximately half that of the typically used Schottky-type FEG (0.3 eV and 0.7 eV, respectively) and can produce a more coherent electron beam. The cold-FEG has been used as a standard electron gun in the material science field for more than 10 years. However, it has not been used for SPA—which requires several thousand to tens of thousands of images/movies with the same quality because it is less stable than Schottky-type FEG, and the quality varies as the recorded images/movies become darker over time by reducing the current. Cold-FEG developed by JEOL provides stable electron beam irradiation over long periods, with only a 10% reduction in brightness over 8 h [31]. Because cryo-EM data collection requires periodic refilling of the liquid nitrogen to the stage and sample loader section, flashing is performed to restore the reduced current over time. After flashing, data collection can begin again, enabling stable imaging of the sample at almost the same quality even with several thousand images. This result predicts that cold-FEG will be indispensable for cryo-EMs and, therefore, used for SPA in the future.

In 2020, Yip *et al.* published the result of a structural analysis using a cryo-EM equipped with a monochromator and an aberration corrector [32]. In that study, they used a monochromator to set the energy spread to 0.1 eV and succeeded in analyzing the structure at 1.25 Å with a lower energy spread than the 0.4 eV of the cold-FEG. At the same time as Yip *et al.*, using the latest Titan Krios equipped with a cold-FEG, a Selectris imaging filter, and a new DED (FalconIV), Nakane *et al.* were able to produce a 1.22 Å resolution structure of apoferritin [33]. Incredibly, they achieved this high-resolution structure from only one and a half days of data collection on the microscope. These results not only established cryo-EM as a tool that can reach atomic resolutions—with more practical machine times—but also demonstrated the capacity of SPA cryo-EM to reconstruct and visualize hydrogen atoms, thereby achieving 'true' atomic resolution reconstructions. Recently, Maki-Yonekura *et al.* using the JEOL CRYOARM300 reached a resolution of 1.19 Å using more than 2 million particle images of apoferritin [34] and remarkably demonstrated the possibility of visualizing the charge of amino acid side chains. Figure 2 shows the differences in the visibility of these world record maps, focusing on tryptophan in each map. The highest resolution map in the database is 1.15 Å, but this is not addressed in this article because the possibility of over-estimation is pointed out in the paper.

Visiting new, learning old

It is worth noting that when technological advances push the limits of what is possible, even older techniques can produce results that exceed previous expectations. For example, in 2015, Fischer *et al.* used FalconI, which cannot take movies, to analyze the structure of the ribosome-EF-Tu complex at 2.9 Å resolution [35]. This result was reported after motion correction proved to be the key to high-resolution structural analysis, and it was higher resolution than the 3.1 Å achieved by film. Furthermore, in 2020–21, Pintilie *et al.* and Danev *et al.* successfully analyzed apoferritin, the most widely used benchmark protein in the SPA cryo-EM workflow, to the resolution of 1.27 and 1.31 Å, respectively. These findings, which were obtained using electron microscope with a Shottky-type FEG, demonstrate that a cold-FEG or monochromator is not necessarily required for reaching atomic resolutions of approximately 1.3 Å [36,37].

Improvement the resolution by software

In addition to hardware development, software advances have been essential for high-resolution structural analysis. In the case of conventional cameras and films, much of the high-resolution information is lost due to various factors inherent with that technology, and it is impossible to retrieve the non-existent high-resolution information by any superior algorithm. Attempts at recovering this lost information via new algorithmic analysis methods were also developed, but the achievable resolutions obtained from these methods did not change significantly.

With the implementation of DEDs, high-resolution information could be recorded, and thus higher-resolution analysis became possible through computational algorithms that analyzed per-particle contrast transfer function (CTF) correction [26], Ewald sphere correction [26,38], anisotropic magnification distortion correction [39,40], beam tilt correction [26] and higher-order aberration correction [40].

Bartesaghi *et al.* re-processed using per-particle motion correction, per-particle CTF correction and dose weight by Frealign to improve their own previously published data of 2.2 to 1.9 Å [41].

Tegunov *et al.* developed the software named 'M' which has a unique algorithm for refinement to improve the resolution from 1.54 to 1.34 Å using deposited apoferritin data on cryo-EM image database EMPIAR-10 248 [42]. The result gives us expect that with higher-resolution data, 1.19 Å by Maki-Yonekura, 1.22 Å by Nakane or 1.25 Å by Yip, M can be used to analyze at higher resolution, e.g. beyond 1 Å.

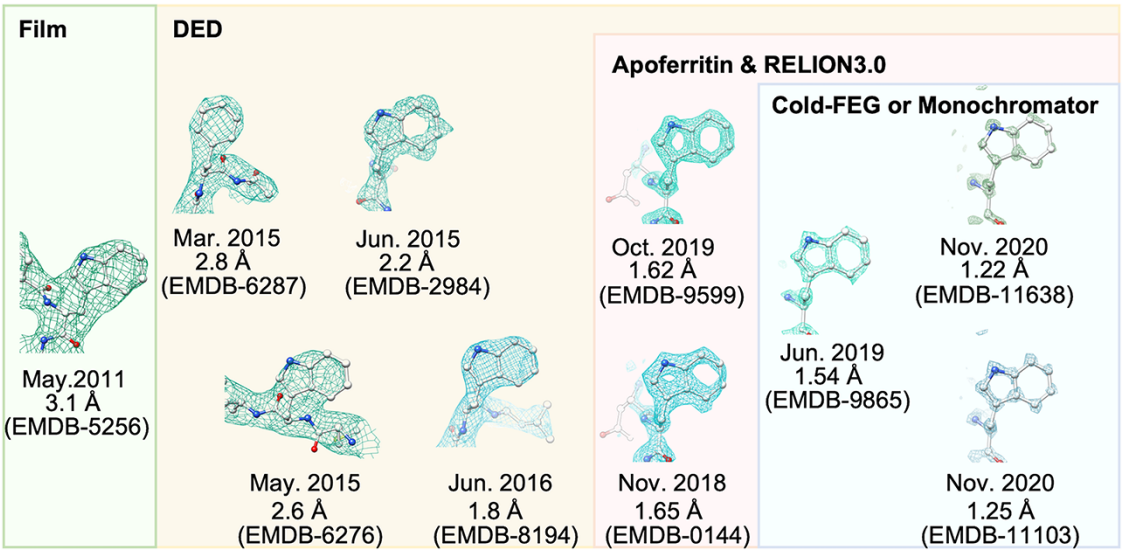

Fig. 2. The highest resolution EM map of all time focused on phenylalanine or tryptophan.

Future perspectives for SPA

SPA cryo-EM has undergone many technological and computational advances in recent years, comparable to those of NMR and X-ray crystallography, and has since developed into a potent tool for high-resolution structural analysis. However, in order to understand the chemical reactions that occur in macromolecules, structural analysis at atomic resolutions must be attainable for the majority of target macromolecules and macromolecular complexes. Unfortunately, most macromolecules are not static and exhibit significant flexibility and dynamic motions that impede high-resolution structural analysis. To date, only analysis with apoferritin, a rigid and symmetrical protein, has resolved structures with resolution range at the atomic level. Therefore, some of the following challenges for atomic resolution structure determination will be, for example, the design and engineering of a stable sample, new sample preparation techniques that produce the best quality of sample embedded in vitreous ice and novel approaches that enable the structural determination of highly dynamic targets.

Cryo-EM for visualizing the heterogeneous specimens

As mentioned above, SPA by cryo-EM enables us to obtain the structures of macromolecular complexes with atomic resolution and contributes to our understanding of mechanisms and function. As the name indicates, the specimens of the SPA are a homogeneous population of purified 'single particles' representing macromolecular complexes or complex assemblies suspended in vitreous ice.

In contrast with SPA method, cryo-ET is another cryo-EM method for 3D structure determination [43,44]. In the cryo-ET, raw tilt images are acquired at the same position by constantly tilting the specimen to $\pm 60^{\circ}$ along with the tilt axis. Then, 3D structure (tomogram) is obtained from aligned tilt-series images by the back-projection method [43,44]. Therefore, cryo-ET can visualize 3D structures of heterogeneous biological specimens such as cells, organelles, bacteria and viruses [44].

In modern-day tomography (cryo-ET), there is a theorem called 'Crowther criterion' to estimate the resolution of the object in the reconstructed tomogram [45]. The Crowther criterion considers in an ideal situation; however, there are several limitations in practical cryo-ET work such as tilt range and electron beam dose amount. Practically, cryo-ET is able to visualize the 3D structure of biological specimens up to $\sim$500 nm thickness with a resolution of approximately 5 nm [46]. However, because the tilt range of the tilt-series image is limited to $\pm 60^{\circ}$, the reconstructed tomogram lacks one-third of the information. Due to the missing wedge, a reconstructed tomogram is slightly stretched to in the Z direction [47]. However, a method known as subtomogram averaging is applied to compensate for the missing information and improve the signal-to-noise ratio (SNR). The resolution of subtomogram representing averaged particles, especially *in situ* macromolecular complexes, has not yet reached a comparable level of resolution to those of SPA. However, recent advances of the cryo-ET methods enable subtomogram averaging to achieve near-atomic resolution. The following section introduces recent advances of cryo-ET methods and the current state of achievable resolutions from subtomogram averaged macromolecular complexes.

Methodological advances

Specimen tilt scheme

In the beginning era of the cryo-ET, the uni-directional (continuous) tilt scheme meaning start of data acquisition, would begin at one end of the tilt range, for example -60° to $+60^{\circ}$, and vice versa, is used for tilt-series images acquisition (Fig. 3a). However, the uni-directional tilt scheme has a problem: images acquired at shallow angle ($\sim \pm 20^{\circ}$) may contain damage due to electron beam irradiation. To reduce the accumulation of beam irradiation damage in images acquired at shallow angles, bi-directional tilt scheme is applied for recording tilt-series images (Fig. 3b). The bi-directional tilt scheme starts recording an image at for example -20° and continues acquiring images until the opposite end of the tilt range $+60^{\circ}$ (Fig. 3b). Then, the specimen is tilted back to

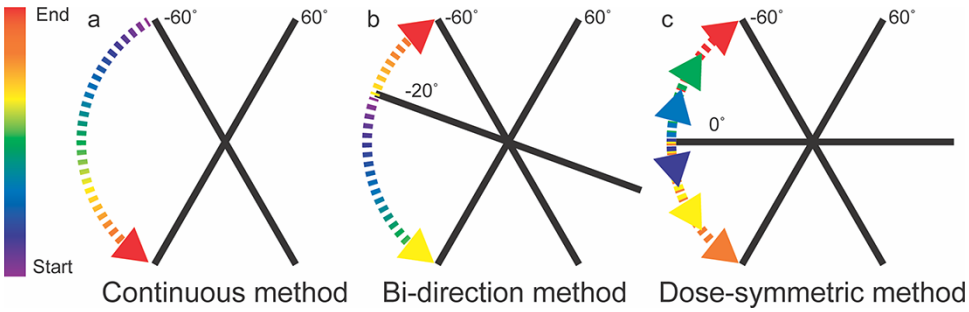

Fig. 3. Schemes of tilt-series acquisition. (a) Continuous method. (b) Bi-directional method. (c) Dose-symmetric method.

−22° and recording images restarts until −60°. The latest tilt scheme is known as a dose-symmetry tilt scheme [48]. The dose-symmetry tilt scheme starts recording at 0°, and then the specimen is tilted to one side and then tilted to the opposite side like a pendulum with increasing the tilt angle (Fig. 3c). Therefore, the dose-symmetry tilt scheme is possible to acquire fresh images at shallow angles. Compared to other resolutions produced by other tilt schemes, the dose-symmetry approach yields the best resolution reconstructions [48,49].

Recently, two notable reports of a hybrid method using SPA and cryo-ET have been developed. One method is known as the TYGRESS (tomography-guided 3D reconstruction of subcellular structures) [50], and the other is hStA (hybrid subtomogram averaging) [51]. With the hybrid approach, a user records a tilt-series using dose-symmetry tilt scheme; however, utilizing the residual electron dose after acquiring a high-dose image of the specimen tilted at 0°. The initial structure of target macromolecule is then obtained by applying subtomogram averaging to the particles chosen from reconstructed tomograms. The geometric information of each particle obtained during particle picking and subtomogram averaging is then used to refine the reconstruction of target structure from particles picked from high-dose images by SPA. These hybrid methods seem to reduce the particle number required for achieving atomic resolution.

Acquisition methods

As with SPA, the more particles number provide spatial resolution in the subtomogram averaging. If the target macromolecular complex has only a small number of copies in cells, the number of tomograms becomes a limiting factor when subtomogram averaging is applied. For example, only 93 particles of tripeptidyl peptidase II were detected in 70 tomograms of the primary cultured hippocampal neuron [52]. Therefore, shortening and efficiency of tilt-series image acquisition time are important for achieving higher resolution from subtomogram averaging.

One of the solutions for shortening of the tilt-series images acquisition time is fast-increment single exposure (FISE) method [53,54]. The idea of the FISE method is recording a long movie file without focus steps and tracking steps in each tilt angle, as subtomogram averaging of *in vitro* 70S ribosome acquired with FISE method. Using this method, resolution reaching 9 Å was achieved, and the image quality was secured [54]. Because the acquisition time of FISE method is limited by the stage stability and higher electron counting speed in camera at present, it is expected that new generations of hardware will enable further faster tilt-series acquisition.

Although acquisition time was shortened by the FISE method, it still acquires tilt-series images one by one. To be efficient in the tilt-series image acquisition, beam image-shift electron cryo-tomography (BISECT) method has recently been developed [55]. The BISECT method applies beam tilt induced image-shift approach combined with SPA. Recently, two other beam image-shift cryo-ET methods named parallel cryo-electron tomography (PACE-tomo) [56] and Multishot tomography [57] are developed. Both PACE-tomo and Multishot tomography have been demonstrated to acquire tilt-series images of not only purified specimens but also focused ion beam (FIB) milled cellular specimens. These beam-image-shift methods efficiently capture high-quality tilt-series images and allow for structural analysis by subtomogram averaging. Bringing the point further, through these new techniques, the resolution of subtomogram averaging from particles derived from FIB milled specimens has now achieved subnanometer [56,57].

Software packages for subtomogram averaging

There are many software packages for subtomogram averaging, each of which has unique features [58]. The improvements to these software packages and workflows have contributed significantly to achieving better resolution [40,59,60]. Despite many options for software packages, one of the most remarkable software packages seems to be an M [42]. The application of M combined with Warp and RELION enabled users to obtain the structure of an *in situ* 70S ribosome with a resolution 3.5 Å, and resolutions achieved in this range are now comparable with those structures derived from SPA (Fig. 4).

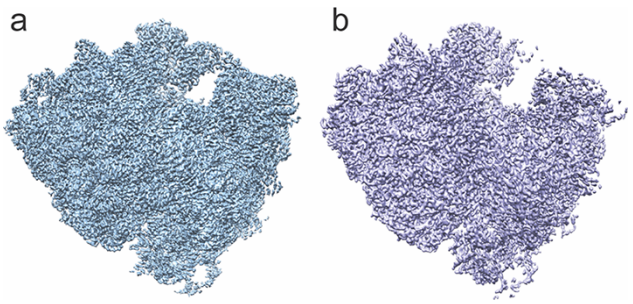

Fig. 4. Structural comparison of 70S ribosome obtained by SPA and subtomogram averaging. (a) SPA of isolated 70S ribosome from *E. coli*. (b) Subtomogram averaging of *in situ* 70S ribosome in *M. pneumoniae*.

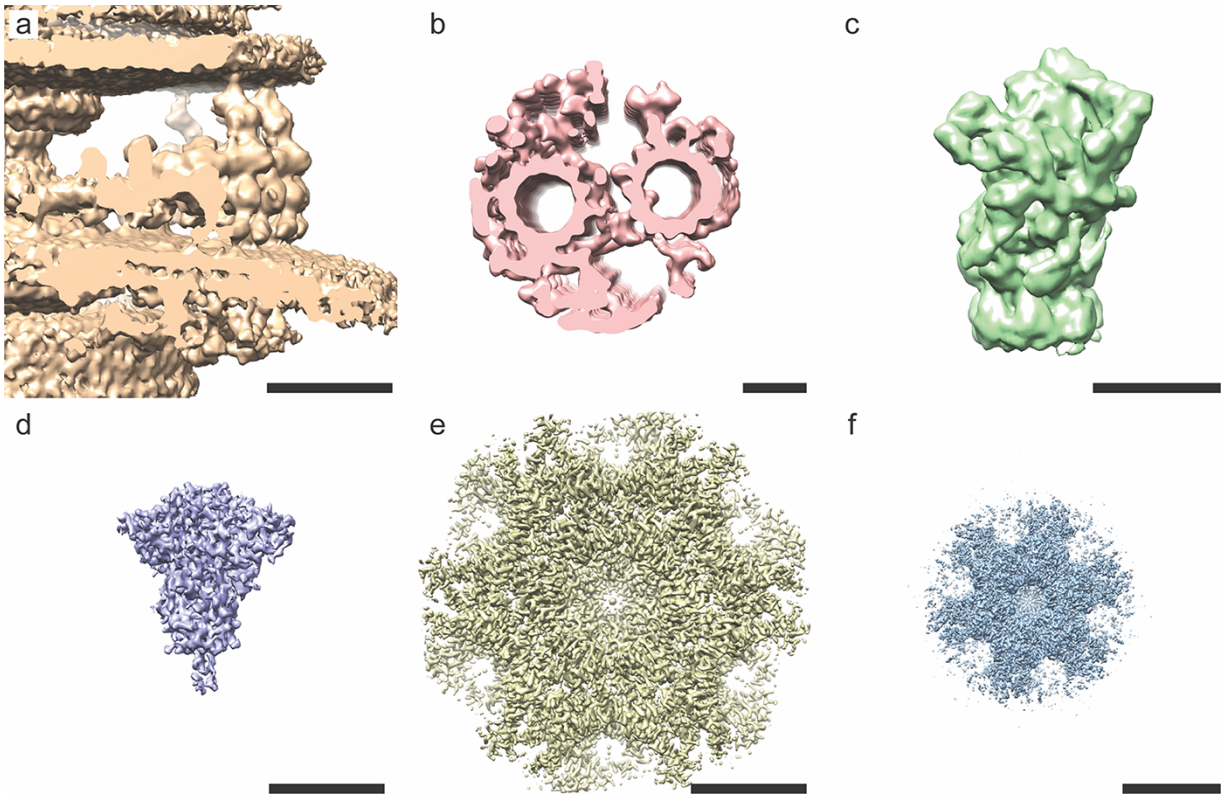

Fig. 5. Panels of recent subtomogram averaged structures of *in situ* macromolecular complexes. (a) *Helicobacter pylori* flagellar motor (EMD-25 123), (b) central pair apparatus WT *Chlamydomonas* (EMD-31 143), (c) 26S proteasome (GS1) (EMD-3916), (d) SRAS CoV-2 spike glycoprotein (EMD-11 222), (e) HIV-1 capsid-SP1 (EMD-11 655), (f) EIAV capsid-spacer-peptide hexamer. Scale bar: 100 Å.

Progress of the resolution of macromolecular complex *in situ*

Cryo-ET and subtomogram averaging have contributed significantly to the exploration of structures from macromolecular complexes *in situ* (Fig. 5). In the following sections, we will discuss subtomogram averaging of several *in situ* macromolecules and introduce key features that directly contributed to their reconstructions.

Flagellar and cilia

The flagellar and cilia are highly sophisticated macromolecular complexes, which convert chemical energy to physical energy. The first subtomogram averaging of *in situ* macromolecular complex was performed on the flagellar motor in *Treponema primitia* [61]. The tilt-series images from that study were recorded with a 300 keV TEM equipped with a CCD camera. Although the averaged map's final resolution was 70 Å, the reconstruction contained the structure of the flagellar motor. By contrast, the current equipment and workflow methods today commonly produce structures of *F* bacterial flagellar motor of approximately 20 Å resolution [62,63].

The motile cilium has a 9 + 2 structure which comprised of an outer doublet microtubule corresponding to '9' and central pair apparatus corresponding to '2'. For an improved resolution, subtomogram averaging of the 9 + 2 structure was averaged individually of one another. This resulted in reconstructing one microtubule from the central pair at ∼23 Å resolution and the central pair apparatus at ∼33 Å [64,65]. Although these resolutions are not relatively high, the combination of structural results with that from genetic modification of the cells makes it possible to identify and annotate the cilium structure by comparisons with wild type.

Viruses

Because of the physical size of viral particles, viral specimens can be much thinner than typical cellular specimens. Therefore, the tilt-series of viral specimens display better SNR and is appropriate for high-resolution subtomogram averaging. The Human Immunodeficiency Virus-1 (HIV-1) lattice is one example and is used for systematically tests of various experimental parameters [49].

The highest resolution of subtomogram averaged viral specimen to date is 2.9 Å resolution reconstruction of Equine infectious anemia virus (EIAV) virus-like particle [66].

Since 2019, worldwide pandemic of severe acute respiratory syndrome coronavirus 2 (SARS-CoV-2) has continued. Essential to the invasion of host cells is the surface protein of SARS-CoV-2, known as the spike protein. Therefore, the spike is a prime target for the neutralizing antibodies. Recently, the structure of SARS-CoV-2 spike protein has been obtained with subtomogram averaging [67,68], and these SARS-CoV-2 spike proteins will contribute to pharmaceutical drug discovery and design.

Proteasome

The 26S proteasome consists of 66 subunits and exhibits different conformations depending on the functional state. The first subtomogram averaging of *in situ* 26S proteasome was

conducted with primary cultured hippocampal neurons [69]. Due to the acquisition of the tilt-series images with the Volta phase plate [70], the 26S proteasome particles are clearly distinguishable in reconstructed tomograms by visual inspection. Furthermore, the subtomogram averaged 19S regulatory particles in the 26S proteasome could be classified into two classes: ground state and substrate processing state. The resolution of the subtomogram averaged 26S proteasome in the ground state and substrate processing state was 27 Å and 31 Å resolution, respectively. As shown in this work, it became possible to correlate the *in situ* localization of the macromolecular complexes and their functional state. Since then, subtomogram averaging of *in situ* macromolecular complexes has become more enthusiastic. The subtomogram averaging of 26S from FIB milled specimens such as *Chlamydomonas* and primary cultured neuronal cells has also produced results with ranges of resolutions capable of determining biological function [71–74].

Ribosome

The ribosome functions as a protein synthesis machine and is critical function for the life. Furthermore, the ribosome exhibits several states, such as the membrane-bound state, polysome state and 100S ribosome (pair of 70S ribosomes). Due to the particle size and molecular weight, both 70S and 80S ribosomes are easily distinguishable from other macromolecular complexes visualized in cellular tomograms by visual inspection. Previously, subtomogram averaging of ribosome particles was carried out by several groups, with reconstructions reaching ∼30 Å resolution [74,75]. Subtomogram averaging of the ribosome has also been carried out with FIB milled specimens for structural analysis of pre-ribosomes in the nucleus [76]. Currently, the highest resolution of the *in situ* 70S ribosome is 3.4 Å in *Mycoplasma pneumoniae* [42]. In *M. pneumoniae* cells, several states have been determined with a subnanometer resolution, such as the 70S ribosome and RNA Polymerase-ribosome supercomplexes [77]. Due to the large copy number of ribosomes within a cell, this has established the ribosome as a benchmark from the cryo-ET workflow, including subtomogram averaging [56,57,78].

Future perspectives cryo-ET and subtomogram averaging

Visualizing macromolecular complexes *in situ* with high resolutions is critical to investigating the details of how and where these macromolecular complexes contribute to biological functions. The cryo-ET and subtomogram averaging had made possible structural and topographic analysis of macromolecular complexes *in situ*. Furthermore, the improved hardware and steady progress of advanced methods for cryo-ET, such as those described from the subtomogram averaged structures of *in situ* macromolecular complexes, have shown that cryo-ET can now achieve near-atomic resolution. However, the targets of subtomogram averaging are still only macromolecular complexes such as ribosome. Therefore, one of the future challenging of the subtomogram averaging seems to be extending the analysis targets to include smaller molecular complexes. Once the targets for the subtomogram averaging are extended to smaller molecular complexes, much more information can be extracted from cellular tomograms.

Due to accumulations of the structural analyses of molecular complexes by X-ray crystallography and SPA, it is possible to search the protein structures by accessing to the Protein Data Bank and the Electron Microscopy Data Bank. However, it is still hard to say that the databases cover all protein complexes formed in cells. Hence, cryo-ET of cellular specimens has a possibility to discover novel protein complexes. The structural analysis of the unknown molecular complexes can be managed by the subtomogram averaging. However, subtomogram averaging is not able to identify the protein complex. Therefore, another future challenging of the cryo-ET and subtomogram averaging is developing a method for identification of the novel protein complexes. Once a method for identification of unknown protein complexes from subtomogram averaged particles was developed, the combination of cryo-ET and the identification method will be a game-changer of structural biology.

Acknowledgements

Authors would like to appreciate Masahide Kikkawa for the critical reading of the manuscript and fruitful discussion.

Funding

This work was partially supported by JSPS KAKENHI Grant-in-Aid for Scientific Research on Innovative Areas JP22K18359 and Grant-in-Aid for Scientific Research (B) JP22H02559 to T.K. and JSPS KAKENHI Grant-in-Aid for Scientific Research on Innovative Areas JP19H05707 and Grant-in-Aid for Sci-entific Research (C) JP19K06594 to Y.F. This work was also supported by JST ERATO Grant Number JPMJER1901 to Y.F. And this research was partially supported by Research Support Project for Life Science and Drug Discovery (Basis for Supporting Innovative Drug Discovery and Life Sci-ence Research (BINDS)) from AMED under Grant Number JP21am0101072 to T.K.

References

1. Velmurugan D, Pachaiappan R, and Ramakrishnan C (2020) Recent trends in drug design and discovery. *Curr. Top. Med. Chem.* 20: 1761–1770.
2. Bai X, Fernandez I, McMullan G, and Scheres S (2013) Ribosome structures to near-atomic resolution from thirty thousand cryo-EM particles. *eLife* 2: e00461.
3. Liao M, Cao E, Julius D, and Cheng Y (2013) Structure of the TRPV1 ion channel determined by electron cryo-microscopy. *Nature* 504: 107–112.
4. Cao E, Liao M, Cheng Y, and Julius D (2013) TRPV1 structures in distinct conformations reveal activation mechanisms. *Nature* 504: 113–118.
5. Kühlbrandt W (2014) Biochemistry. The resolution revolution. *Science* 343: 1443–1444.
6. McMullan G, Chen S, Henderson R, and Faruqi A (2009) Detective quantum efficiency of electron area detectors in electron microscopy. *Ultramicroscopy* 109: 1126–1143.
7. Milazzo A, Moldovan G, Lanman J, Jin L, Bouwer J, Klienfelder S, Peltier S, Ellisman M, Kirkland A, and Xuong N (2010) Characterization of a direct detection device imaging camera for transmission electron microscopy. *Ultramicroscopy* 110: 744–747.
8. Bammes B, Rochat R, Jakana J, Chen D, and Chiu W (2012) Direct electron detection yields cryo-EM reconstructions at resolutions beyond 3/4 Nyquist frequency. *J. Struct. Biol.* 177: 589–601.
9. Jin L and Bilhorn R (2010) Performance of the DDD as a direct electron detector for low dose electron microscopy. *Microsc. Microanal.* 16: 854–855.

10. Glaeser R (2008) Retrospective: radiation damage and its associated "information limitations". *J. Struct. Biol.* 163: 271–276.
11. Brilot A, Chen J, Cheng A, Pan J, Harrison S, Potter C, Carragher B, Henderson R, and Grigorieff N (2012) Beam-induced motion of vitrified specimen on holey carbon film. *J. Struct. Biol.* 177: 630–637.
12. Henderson R and Glaeser R (1985) Quantitative analysis of image contrast in electron micrographs of beam-sensitive crystals. *Ultramicroscopy* 16: 139–150.
13. Böttcher B (1995) Electron cryo-microscopy of graphite in amorphous ice. *Ultramicroscopy* 58: 417–424.
14. Bullough P and Henderson R (1997) Use of spot-scan procedure for recording low-dose micrographs of beam-sensitive specimens. *Ultramicroscopy* 21: 223–230.
15. Downing K (1991) Spot-scan imaging in transmission electron microscopy. *Science* 251: 53–59.
16. Glaeser R and Hall R (2011) Reaching the information limit in cryo-EM of biological macromolecules: experimental aspects. *Biophys. J.* 100: 2331–2337.
17. Glaeser R, McMullan G, Faruqi A, and Henderson R (2011) Images of paraffin monolayer crystals with perfect contrast: minimization of beam-induced specimen motion. *Ultramicroscopy* 111: 90–100.
18. Campbell M, Cheng A, Brilot A, Moeller A, Lyumkis D, Veesler D, Pan J, Harrison S, Potter C, Carragher B, and Grigorieff N (2012) Movies of ice-embedded particles enhance resolution in electron cryo-microscopy. *Structure* 20: 1823–1828.
19. Li X, Mooney P, Zheng S, Booth C, Braunfeld M, Gubbens S, Agard D, and Cheng Y (2013) Electron counting and beam-induced motion correction enable near-atomic-resolution single-particle cryo-EM. *Nat. Methods* 10: 584–590.
20. Scheres S (2014) Beam-induced motion correction for sub-megadalton cryo-EM particles. *eLife* 3: e03665.
21. Yu X, Ge P, Jiang J, Atanasov I, and Zhou Z (2011) Atomic model of CPV reveals the mechanism used by this single-shelled virus to economically carry out functions conserved in multishelled reoviruses. *Structure* 19: 652–661.
22. Campbell M, Veesler D, Cheng A, Potter C, and Carragher B (2015) 2.8 Å resolution reconstruction of the thermoplasma acidophilum 20S proteasome using cryo-electron microscopy. *eLife* 4: e06380.
23. Grant T and Grigorieff N (2015) Measuring the optimal exposure for single particle cryo-EM using a 2.6 Å reconstruction of rotavirus VP6. *eLife* 4: e06980.
24. Bartesaghi A, Merk A, Banerjee S, Matthies D, Wu X, Milne J, and Subramaniam S (2015) 2.2 Å resolution cryo-EM structure of β-galactosidase in complex with a cell-permeant inhibitor. *Science* 348: 1147–1151.
25. Merk A, Bartesaghi A, Banerjee S, Falconieri V, Rao P, Davis M, Pragani R, Boxer M, Earl L, Milne J, and Subramaniam S (2016) Breaking cryo-EM resolution barriers to facilitate drug discovery. *Cell* 165: 1698–1707.
26. Zivanov J, Nakane T, Forsberg B, Kimanius D, Hagen W, Lindahl E, and Scheres S (2018) New tools for automated high-resolution cryo-EM structure determination in RELION-3. *eLife* 7: e42166.
27. Danev R, Yanagisawa H, and Kikkawa M (2019) Cryo-electron microscopy methodology: current aspects and future directions. *Trends Biochem. Sci.* 44: 837–848.
28. Xie Q, Yoshioka C, and Chapman M (2020) Adeno-associated virus (AAV-DJ)-cryo-EM structure at 1.56 Å resolution. *Viruses* 12: 1194.
29. Kato T, Makino F, Nakane T, Terahara N, Kaneko T, Shimizu Y, Motoki S, Ishikawa I, Yonekura K, and Namba K (2019) CryoTEM with a cold field emission gun that moves structural biology into a new stage. *Microsc. Microanal.* 25: 998–999.
30. Hamaguchi T, Maki-Yonekura S, Naitow H, Matsuura Y, Ishikawa T, and Yonekura K (2019) A new cryo-EM system for single particle analysis. *J. Struct. Biol.* 207: 40–48.
31. Jumbo Y, Hashiguchi H, and Ohnishi I (2020) Development of JEM-ARM300F2: an aberratin corrected 300 kV microscope capable of both ultrahigh spatial resolution imaging and highly sensitive analysis over a wide range of acceleration voltage. *JEOL NEWS* 55: 43–48.
32. Yip K, Fischer N, Paknia E, Chari A, and Stark H (2020) Atomic-resolution protein structure determination by cryo-EM. *Nature* 587: 157–161.
33. Nakane T, Kotecha A, Sente A, McMullan G, Masiulis S, Brown P, Grigoras I, Malinauskaite L, Malinauskas T, Miehling J, Uchański T, Yu L, Karia D, Pechnikova E, de Jong E, Keizer J, Bischoff M, McCormack J, Tiemeijer P, Hardwick S, Chirgadze D, Murshudov G, Aricescu A, and Scheres S (2020) Single-particle cryo-EM at atomic resolution. *Nature* 587: 152–156.
34. Maki-Yonekura S, Kawakami K, Hamaguchi T, Takaba K, and Yonekura K (2021) Hydrogen properties and charges in a sub-1.2 Å resolution cryo-EM structure revealed by a cold field emission beam. *bioRxiv*. 10.1101/2021.12.21.473430.
35. Fischer N, Neumann P, Konevega A L, Bock L V, Ficner R, Rodnina M V, and Stark H (2015) Structure of the *E. coli* ribosome-EF-Tu complex at <3 Å resolution by Cs-corrected cryo-EM. *Nature* 520: 567–570.
36. Zhang K, Pintilie G, Li S, Schmid M, and Chiu W (2020) Resolving individual atoms of protein complex by cryo-electron microscopy. *Cell Res.* 30: 1136–1139.
37. Danev R, Yanagisawa H, and Kikkawa M (2021) Cryo-EM performance testing of hardware and data acquisition strategies. *Microscopy* 70: 487–497.
38. Wolf M, DeRosier D, and Grigorieff N (2006) Ewald sphere correction for single-particle electron microscopy. *Ultramicroscopy* 106: 376–382.
39. Grant T and Grigorieff N (2015) Automatic estimation and correction of anisotropic magnification distortion in electron microscopes. *J. Struct. Biol.* 192: 204–208.
40. Zivanov J, Otyn J, Ke Z, Qu K, Morado D, CastaCo-Diez D, von Kügelgen A, Bharat T, Briggs J, and Scheres S (2022) A Bayesian approach to single-particle electron cryo-tomography in RELION-4.0. *bioRxiv*. 10.1101/2022.02.28.482229.
41. Bartesaghi A, Aguerrebere C, Falconieri V, Banerjee S, Earl L, Zhu X, Grigorieff N, Milne J, Sapiro G, Wu X, and Subramaniam S (2018) Atomic resolution cryo-EM structure of β-galactosidase. *Structure* 26: 848–856.e3.
42. Tegunov D, Xue L, Dienemann C, Cramer P, and Mahamid J (2021) Multi-particle cryo-EM refinement with M visualizes ribosome-antibiotic complex at 3.5 Å in cells. *Nat. Methods* 18: 186–193.
43. Baumeister W (2005) From proteomic inventory to architecture. *FEBS Lett.* 579: 933–937.
44. Turk M and Baumeister W (2020) The promise and the challenge of cryo-electron tomography. *FEBS Lett.* 594: 3243–3261.
45. Crowther R A, DeRosier D J, and Klug A (1970) The reconstruction of a three-dimensional structure from its projections and its applications to electron microscopy. *Procs. Royal Soc.* 317: 319–340.
46. Briggs J A G (2013) Structural biology *in situ* – the potential of subtomogram averaging. *Curr. Opin. Struct. Biol.* 23: 261–267.
47. Fukuda Y, Laugks U, Lučić V, Baumeister W, and Danev R (2015) Electron cryotomography of vitrified cells with a Volta phase plate. *J. Struct. Biol.* 190: 143–154.
48. Hagen W J H, Wan W, and Briggs J A G (2017) Implementation of a cryo-electron tomography tilt-scheme optimized for high resolution subtomogram averaging. *J. Struct. Biol.* 197: 191–198.
49. Turoňová B, Hagen W J H, Obr M, Mosalaganti S, Beugelink J W, Zimmerli C E, Kräusslich H-G, and Beck M (2020) Benchmarking tomographic acquisition schemes for high-resolution structural biology. *Nat. Commun.* 11: 876.

50. Song K, Shang Z, Fu X, Lou X, Grigorieff N, and Nicastro D (2020) *In situ* structure determination at nanometer resolution using TYGRESS. *Nat. Methods* 17: 201–208.
51. Sanchez R M, Zhang Y, Chen W, Dietrich L, and Kudryashev M (2020) Subnanometer-resolution structure determination in situ by hybrid subtomogram averaging – single particle cryo-EM. *Nat. Commun.* 11: 3709.
52. Fukuda Y, Beck F, Plitzko J M, and Baumeister W (2017) In situ structural studies of tripeptidyl peptidase II (TPPII) reveal spatial association with proteasomes. *Proc. Natl Acad. Sci. U. S. A.* 114: 4412–4417.
53. Chreifi G, Chen S, Metskas L A, Kalplan M, and Jensen G J (2019) Rapid tilt-series acquisition for electron cryotomography. *J. Struct. Biol.* 205: 163–169.
54. Eisenstein F, Danev R, and Pilhofer M (2019) Improved applicability and robustness of fast cryo-electron tomography data acquisition. *J. Struct. Biol.* 208: 107–114.
55. Bouvette J, Liu H-F, Du X, Zhou Y, Sikkema A P, da Fonseca Rezende E Mello J, Klemm B P, Huang R, Schaaper R M, Borgnia M J, and Bartesaghi A (2021) Beam image-shift accelerated data acquisition for near-atomic resolution single-particle cryo-electron tomography. *Nat. Commun.* 12: 1957.
56. Eisenstein F, Yanagisawa H, Kashihara H, Kikkawa M, Tsukita S, and Danev R (2022) Parallel cryo electron tomography on *in situ* lamellae. *bioRxiv*. 10.1101/2022.04.07.487557.
57. Khavnekar S, Wan W, Mujunder P, Wietrzynski W, Erdmann P S, and Plitzko J M (2022) Multishot tomography for high-resolution in situ subtomogram averaging. *bioRxiv*. 10.1101/2022.04.10.487763.
58. Zhang P (2019) Advances in cryo-electron tomography and subtomogram averaging and classification. *Curr. Opin. Struct. Biol* 58: 249–258.
59. Burt A, Gaifas L, Dendooven T, and Gutsche I (2021) A flexible framework for multi-particle refinement in cryo-electron tomography. *PLoS Biol.* 19: e3001319.
60. Ni T, Frosio T, Mendonca L, Sheng Y, Clare D, Himes B A, and Zhang P (2022) High-resolution in situ structure determination by cryo-electron tomography and subtomogram averaging using emClarity. *Nat. Protoc.* 17: 421–444.
61. Murphy G E, Leadbetter J R, and Jensen G J (2006) *In situ* structure of the complete *Treponema primitia* flagellar motor. *Nature* 442: 1062–1064.
62. Chang Y, Zhang K, Carrol B L, Zhao X, Charon N W, Noris S J, Motaleb M A, Li C, and Liu J (2020) Molecular mechanism for rotational switching of the bacterial flagellar motor. *Nat. Struct. Mol. Biol.* 27: 1041–1047.
63. Tachiyama S, Chan K L, Liu X, Hathroubi S, Li W, Peterson B, Khan M F, Ottermann K M, Liu J, and Roujeinikova A (2022) The flagellar motor protein FliL forms a scaffold of circumferentially positioned rings required for stator activation. *Proc. Natl Acad. Sci. U. S. A.* 119: e2118401119.
64. Cai K, Zhao Y, Zhao L, Phan N, Hou Y, Cheng X, Witman G B, and Nicastro D (2021) Structural organization of the C1b projection within the ciliary central apparatus. *J. Cell Sci.* 134: jcs254227.
65. Hou Y, Zhao L, Kubo T, Cheng X, McNeill N, Oda T, and Witman G B (2021) *Chlamydomonas* FAP70 is a component of the previously uncharacterized ciliary central apparatus projection C2a. *J. Cell Sci.* 134: jcs258540.
66. Obr M, Hagen W J H, Dick R A, Yu L, Kotecha A, and Schur F K (2022) Exploring high-resolution cryo-ET and subtomogram averaging capabilities of contemporaly DEDs. *J. Struct. Biol.* 214: 107852.
67. Ke Z, Oton J, Qu K, Cortese M, Zila V, McKeane L, Nakane T, Zivanov J, Neufeldt C, Cerikan B, Lu J M, Peukes J, Xiong X, Kräusslich H G, Scheres S H W, Bartenschlager R, and Briggs J A G (2020) Structures and distribution of SARS-CoV-2 spike proteins on intact virions. *Nature* 588: 498–502.
68. Turoňová B, Sikora M, Schürmann C, Hagen W J H, Welsch S, Blanc F E C, von Bülow S, Gecht M, Bagola K, Hörner C, van Zandbergen G, Landry J, de Azevedo N T D, Mosalaganti S, Schwarz A, Covino R, Mühlebach M D, Hummer G, Locker J K, and Beck M (2020) In situ structural analysis of SARS-CoV-2 spike reveals flexibility mediated by three hinges. *Science* 370: 203–208.
69. Asano S, Fukuda Y, Beck F, Aufderheide A, Förster F, Danev R, and Baumeister W (2015) A molecular census of 26S proteasomes in intact neurons. *Science* 347: 439–442.
70. Danev R, Buijsse B, Khoshouei M, Plitzko J M, and Baumeister W (2014) Volta potential phase plate for in-focus phase contrast transmission electron microscopy. *Proc. Natl. Acad. Sci. U. S. A.* 111: 15635–15640.
71. Albert S, Schaffer M, Beck F, Mosalaganti S, Asano S, Thomas H F, Plitzko J M, Beck M, Baumeister W, and Engel B D (2017) Proteasomes tether to two distinct sites at the nuclear pore complex. *Proc. Natl Acad. Sci. USA* 114: 13726–13731.
72. Guo Q, Lehmer C, Martinez-Sanches A, Rudack T, Beck F, Hartmann H, Perez-Berlanga M, Frottin F, Hipp M S, Hartl U, Edbauer D, Baumeister W, and Fernandez-Busnadiego R (2018) In situ structure of neuronal C9orf72 poly-GA aggregates reveals proteasome recruitment. *Cell* 172: 696–705.
73. Riemenscneider H, Guo Q, Bader J, Frottin F, Farny D, Kleinberger G, Haass C, Mann M, Hartl F U, Baumeister W, Hipp M S, Meissner F, Fernandez-Busnadiego R, and Edbauer D (2022) Gel-like inclusions of C-terminal fragments of TDP-43 sequester stalled proteasomes in neurons. *EMBO Rep.* 19: e53890.
74. Ortiz J O, Brandt F, Matias V R F, Sennels L, Rappsilber J, Scheres S H W, Eibauer M, Hartl F U, and Baumeister W (2010) Structure of hibernating ribosomes studied by cryoelectron tomography in vitro and in situ. *J. Cell Biol.* 190: 613–621.
75. Brandt F, Carlson L A, Hartl F U, Baumeister W, and Grünewald K (2010) The three-dimensional organization of polysomes in intact human cells. *Mol. Cell* 39: 560–569.
76. Erdmann P S, Hou Z, Klumpe S, Khavnekar S, Beck F, Wilfling F, Plitzko J M, and Baumeister W (2021) In situ cryo-electron tomography reveals gradient organization of ribosome biogenesis in intact nucleoli. *Nat. Commun.* 12: 5346.
77. O'Reilly F J, Xue L, Graziadei A, Sinn L, Lenz S, Tegunov D, Blötz C, Singh N, Hagen W J H, Cramer P, Stülke J, Mahamid J, and Rappsilber J (2020) In-cell architecture of an activity transcribing-translating expressome. *Science* 369: 554–557.
78. Klumpe S, Fung H K H, Goetz S K, Zagoriy I, Hampoelz B, Zhang X, Erdmann P S, Baumbach J, Müller C W, Beck M, Plitzko J M, and Mahamid J (2021) A modular platform for automated cryo-FIB workflows. *eLife* 10: e70506.